Learning Rich Features at High-Speed for Single-Shot Object Detection

Tiancai Wang[1*†], Rao Muhammad Anwer[2*], Hisham Cholakkal[2], Fahad Shahbaz Khan[2]
Yanwei Pang[1‡], Ling Shao[2]
[1]School of Electrical and Information Engineering, Tianjin University
[2]Inception Institute of Artificial Intelligence (IIAI), UAE
[1]{wangtc,pyw}@tju.edu.cn, [2]{rao.anwer,hisham.cholakkal,fahad.khan,ling.shao}@inceptioniai.org

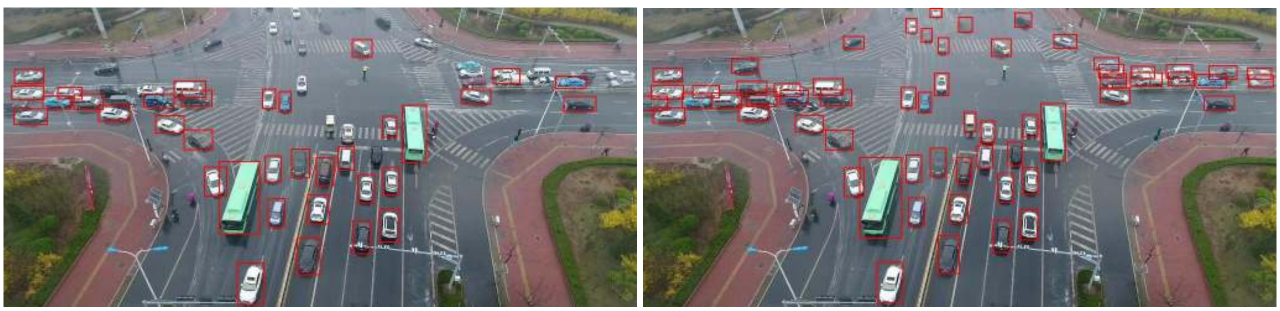

a: RetinaNet (ResNet-101-FPN) [18] b: Our Approach (VGG-16)

Figure 1: Qualitative detection results on an example image from UAVDT dataset [9]. (a) RetinaNet [18], using the powerful ResNet-101-FPN backbone and (b) our detector, using the VGG-16 backbone under similar training and testing scale. Our detector accurately detects *all* 61 vehicle (car, bus and truck) instances, including 45 small vehicles (defined as per MS COCO criteria [19]), while operating at 91 frames per second (FPS) on a single Titan X GPU. See Fig. 5 for more examples.

Abstract

Single-stage object detection methods have received significant attention recently due to their characteristic real-time capabilities and high detection accuracies. Generally, most existing single-stage detectors follow two common practices: they employ a network backbone that is pre-trained on ImageNet for the classification task and use a top-down feature pyramid representation for handling scale variations. Contrary to common pre-training strategy, recent works have demonstrated the benefits of training from scratch to reduce the task gap between classification and localization, especially at high overlap thresholds. However, detection models trained from scratch require significantly longer training time compared to their typical fine-tuning based counterparts. We introduce a single-stage detection framework that combines the advantages of both fine-tuning pre-trained models and training from scratch. Our framework constitutes a standard network that uses a pre-trained backbone and a parallel light-weight auxiliary network trained from scratch. Further, we argue that the commonly used top-down pyramid representation only focuses on passing high-level semantics from the top layers to bottom layers. We introduce a bi-directional network that efficiently circulates both low-/mid-level and high-level semantic information in the detection framework.

Experiments are performed on MS COCO and UAVDT datasets. Compared to the baseline, our detector achieves an absolute gain of 7.4% and 4.2% in average precision (AP) on MS COCO and UAVDT datasets, respectively using VGG backbone. For a 300×300 input on the MS COCO test set, our detector with ResNet backbone surpasses existing single-stage detection methods for single-scale inference achieving 34.3 AP, while operating at an inference time of 19 milliseconds on a single Titan X GPU. Code is available at `https://github.com/vaesl/LRF-Net.`

1. Introduction

Recent years have witnessed significant improvements in detection performance thanks to the advances of deep learning, especially convolutional neural networks (CNNs) [34, 23, 25, 22, 6]. Modern detectors can be divided into two categories: (i) single-stage methods [21, 26, 27, 28, 3, 4] and

*Equal contribution
†Work done at IIAI during Tiancai's internship.
‡Corresponding author

(ii) two-stage approaches [29, 17, 14, 11, 31]. Generally, two-stage methods dominate accuracy whereas the main advantage of single-stage approaches is their high speed [15].

Recent single-stage detectors [18, 36] aim at matching the detection accuracy of more complex two-stage detection methods. Despite showing impressive results on large and medium sized objects, these detectors achieve below-expected performance on small objects [1]. For instance, when using a $\sim 500\times500$ input, state-of-the-art single-stage RetinaNet [18] obtains impressive results with a COCO AP of 47 on large sized objects but only achieves a COCO AP of 14 on small sized objects (defined as in [19]). Small object detection is a challenging problem and requires both low-/mid-level information for accurate object delineation and high-level semantics to differentiate the target object from the background or other object categories.

State-of-the-art single-stage methods [18, 36, 4] typically employ a deeper network backbone (*e.g.*, VGG or ResNet) that is pre-trained on ImageNet dataset [30] for the classification task. These detection frameworks then fine-tune the pre-trained network backbones on the target object detection dataset, leading to faster convergence. However, there is still a task gap between classification-based pre-trained models and the target localization goal influencing the performance at high box overlap thresholds [12]. Recent works [12, 38] have shown that training detection models from scratch counters this issue, leading to accurate localization. While promising, training very deep networks from scratch requires significantly longer training time compared to their typical fine-tuning based counterparts. In this work, we combine the advantages of both pre-training and learning from scratch by introducing a detection framework constituting a standard network that uses a pre-trained backbone and a shallow auxiliary network trained from scratch. The auxiliary network provides complementary low-/mid-level information to the standard pre-trained network, and is especially useful for small and medium objects.

As discussed earlier, both low-/mid-level information and high-level semantics are desired when detecting objects of varying scales, especially small objects. Modern object detectors generally use a top-down pyramidal feature representation [17, 18], where high-level information from top or later layers is fused to semantically weaker high-resolution features in bottom or former layers. Although, such a top-down feature pyramid representation results in improved performance, it only injects high-level semantics to former layers. Further, such a pyramid representation [17] is constructed by the fusion of many layers in a layer-by-layer fashion. In this work, we argue that fusion of high-level information to former layers and low-/mid-level information to later layers is crucial for multi-scale object detection.

Contributions: We propose a single-stage detection approach with the following contributions. First, we introduce

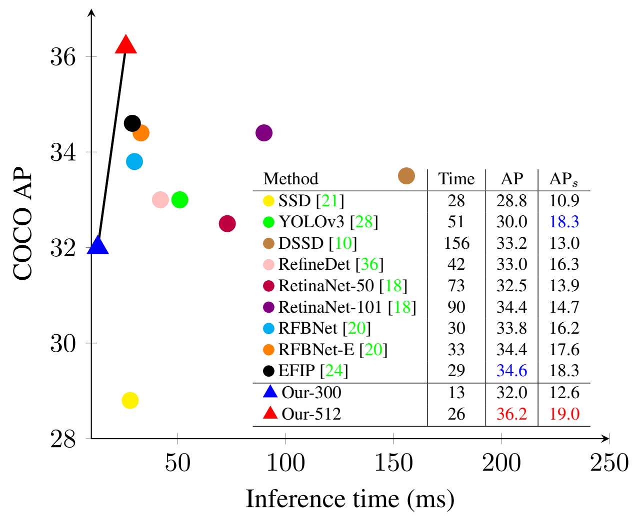

Figure 2: Accuracy (AP) vs. speed (ms) comparison with existing single-stage methods on the MS COCO test-dev. We report both overall accuracy (AP) and performance on small objects (AP$_s$). Our two variants (red and blue triangles) have all the same settings, except for different input sizes (300×300 and 512×512). Here, existing detectors use an input image size of $\sim 512\times512$, except YOLOv3 (608×608). Similar to our approach, most methods [21, 36, 20, 24] here employ VGG backbone. For fair comparison, the speed is measured on a single Titan X GPU. The top two results are marked in red and blue, respectively.

a light-weight scratch network (LSN) that is trained from scratch taking a downsampled image as input and passing it through a few convolutional layers to efficiently construct low-/mid-level features. These low-/mid-level features are then injected into the standard detection network with the pre-trained backbone. Further, we introduce a bi-directional network that circulates both low-/mid-level and high-level semantic information within the detection network.

Experiments are performed on two datasets: MS COCO and Unmanned Aerial Vehicle (UAVDT). On both datasets, our approach achieves superior performance, without any bells and whistles, compared to existing single-stage detection methods. Further, our detector significantly improves the baseline [21] on small objects, with an absolute gain of 8.1% in terms of COCO style AP on the MS COCO dataset. For a 512×512 input, our detector achieves a COCO style AP of 36.2, with an inference time of 26 millisecond (ms), outperforming existing single-stage methods using a similar backbone (VGG) on MS COCO (See Fig. 2).

2. Baseline Fast Detection Framework

In this work, we adopt the popular SSD framework [21] as our baseline due to its combined advantage of high speed and detection accuracy. The standard SSD employs a VGG-

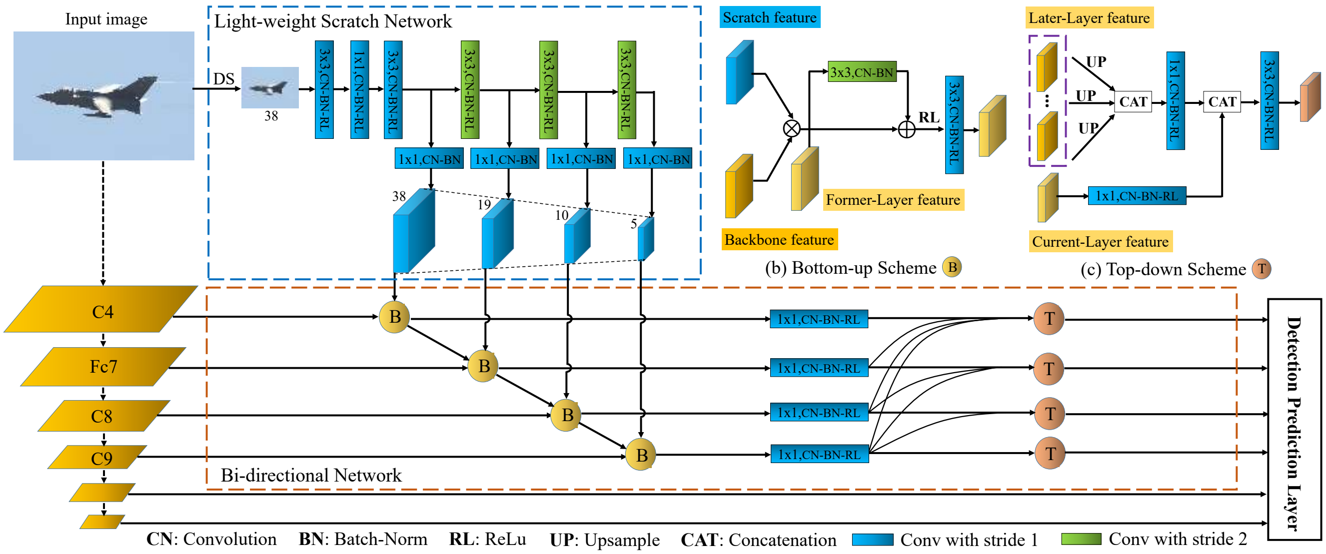

(a) Overall architecture of our proposed detector

Figure 3: (a) Overall architecture of the proposed single-stage object detection method. Our approach consists of three components: the standard SSD network, the light-weight scratch network (LSN) and bi-directional network. Within our LSN, an input image is first downsampled and then passed through light-weight serial operations (LSO) to produce LSN features. Our bi-directional network consists of bottom-up (b) and top-down (c) schemes to circulate both low-/mid-level and high-level semantic information within the network.

16 architecture as the backbone network where layers of different resolutions are used to perform independent predictions. The SSD starts from the $conv4\_3$ layer and further includes the FC_7 (converted into a conv layer) layer from the original VGG-16 network while truncating the last fully connected (FC) layer of the network. It then adds several progressively smaller conv layers, namely $conv8\_2$, $conv9\_2$, $conv10\_2$, and $conv11\_2$ at the end for predictions. The standard SSD employs a feature pyramid hierarchy with former layers (*e.g.*, $conv4\_3$) designated for small object detection whereas later or deep layers (*e.g.*, $conv9\_2$) are assigned with the task of localizing large object instances. The pyramidal hierarchical structure therefore ensures that multi-scale features from different SSD layers are utilized to predict both class scores and bounding boxes. Finally, NMS based post processing strategy is used during inference to obtain final predictions.

Limitations: As discussed above, the standard SSD employs a pyramidal feature hierarchy where independent predictions are performed at layers of different resolutions. However, such a pyramidal representation struggles with large scale variations, especially to detect small sized objects. This is likely due to the limited semantic information in the former layers (*e.g.*, $conv4\_3$) of the SSD, compared to the later layers [15]. Further, the pyramidal feature hierarchy in the standard SSD starts from high up the network, *e.g.*, $conv4\_3$ layer in case of VGG-16. Prior works have addressed the importance of both shallow and high-level semantic information for detecting small objects [17]. Most common solutions to this problem include *e.g.*, large-scale context [10], better feature extraction by deepening the model [10, 18], featurized image pyramids [24] and top-down feature pyramid representation to inject high-level semantics to former layers [18, 35, 37]. The featurized image pyramids strategy [24] does not provide high-level semantics to former layers whereas top-down pyramid scheme does not explicitly distribute low-/mid-level complementary information to later layers of the network. Further, solutions involving deepening the model and large-scale context improve the performance at the cost of computational speed.

3. Our Approach

In this section, we first present our overall detection architecture and introduce our light-weight scratch network (LSN) (sec. 3.1) to integrate complementary information in the standard SSD prediction layers. We then describe our bi-directional network (sec. 3.2) designed to circulate both low-/mid-level and high-level semantic information within the detection network.

Overall Architecture: Fig. 3 (a) shows the overall architecture consisting of three main components: the standard SSD network, light-weight scratch network (LSN) and bi-directional network. As discussed earlier, standard SSD employs a pre-trained network backbone. We therefore term the features from standard SSD layers ($conv4\_3$,

FC_7, $conv8\_2$, $conv9\_2$, $conv10\_2$, and $conv11\_2$) as backbone features since they originate from the pre-trained network backbone. Similar to [21], we employ VGG-16 as the backbone network. The light-weight scratch network (LSN) produces a low-/mid-level feature representation which is then injected into the backbone features of subsequent standard prediction layers to improve their performance. Afterwards, the resulting features from the current and former layers are combined in the bottom-up fashion inside our bi-directional network. The top-down scheme in our bi-directional network contains independent parallel connections to inject high-level semantic information from later layers to former layers of the network.

Our bi-directional network has the following differences compared to the feature pyramid network (FPN) [17] employed in several existing single-stage detectors [18, 36]. First, the bottom-up part of FPN follows the CNN's pyramidal feature hierarchy which is also used in the standard SSD framework. Both the bottom-up part of FPN and SSD follow the feed-forward computation of backbone network which builds a feature hierarchy. In addition to the bottom-up part in FPN/standard SSD, the bottom-up scheme in our bi-directional network propagates features from the former to later layers in a cascaded fashion. Moreover, the top-down pyramid in FPN performs a layer-by-layer fusion of many CNN layers through cascaded operations. Instead of cascaded/sequential layer-by-layer fusion, the prediction layers are fused through independent parallel connections in the top-down scheme of our bi-directional network.

3.1. Light-Weight Scratch Network

Our light-weight scratch network (LSN) is simple, tightly linked to the standard SSD prediction layers and is used to construct low-/mid-level feature representations, termed as LSN features. We present the feature extraction strategy used in our LSN followed by a description of the LSN architecture.

LSN Feature Extraction: The feature extraction strategy commonly employed in existing detection frameworks involves extracting features from the network backbone, such as VGG-16, in a repeated stack of multiple convolutional blocks and max-pooling layers to produce semantically strong features (see Fig. 4 (a)). Such a feature extraction strategy is beneficial for the task of image classification that prefers translation invariance. Different from image classification, object detection also requires accurate object delineation for which local low-/mid-level feature (*e.g.*, texture) information is also crucial [38]. To compensate the loss of information in the backbone features from the pre-trained network, an alternative feature extraction scheme is utilized in our LSN, as shown in Fig. 4 (b). First, an input image is downsampled by a pooling operation to the target size of first SSD prediction layer. The resulting downsampled image is then passed through light-weight serial operations (LSO) including convolution, batch-norm and ReLU layers. Note that our LSN is trained from scratch with random initialization. It follows a similar pyramidal feature hierarchy, as in standard SSD, which is constructed as

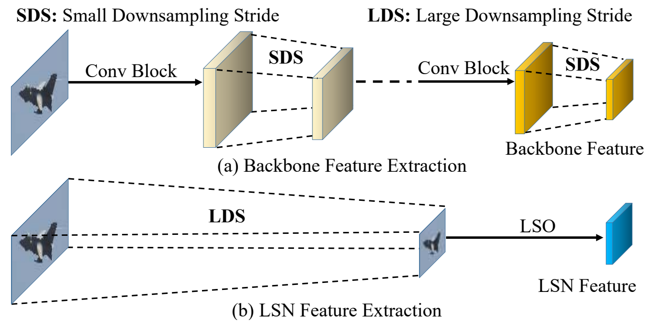

Figure 4: (a) Standard SSD feature extraction employs several convolution blocks together with small downsampling strides. (b) In our LSN, the input image is first downsampled to the target size followed by light-weight serial operations (LSO) to produce LSN features.

$$S_p = \{s_1, s_2, \ldots, s_n\} \tag{1}$$

where n is the number of feature pyramid levels selected to match the size of standard SSD prediction layers. We start by downsampling the input image I to the target size of first SSD prediction layer (down-sampling rate is 8 in our case). Then, we use the resulting downsampled image I_t to generate the initial LSN feature $s_{int(0)}$:

$$s_{int(0)} = \varphi_{int(0)}(I_t) \tag{2}$$

where $\varphi_{int(0)}$ denotes the serial operations, including one 3×3 and one 1×1 conv. block. The initial feature $s_{int(0)}$ is then used to generate an intermediate feature set s_{int}. The k^{th} intermediate feature is obtained using $(k-1)^{th}$ intermediate feature:

$$s_{int(k)} = \varphi_{int(k)}(s_{int(k-1)}) \tag{3}$$

where $k = (1, \ldots, n)$ and $\varphi_{int(k)}(.)$ denotes one 3×3 conv. block. When $k = 1$, the $(k-1)^{th}$ intermediate feature is equal to the initial LSN feature. Next, we apply a 1×1 conv. block to the k^{th} level intermediate feature to generate the k^{th} level LSN feature of S_p,

$$s_k = \varphi_{trans(k)}(s_{int(k)}) \tag{4}$$

where $\varphi_{trans(k)}(.)$ denotes a 1×1 conv. block that transforms the LSN feature channels to match the corresponding standard SSD feature.

3.2. Bi-directional Network

The bi-directional network circulates both low-/mid-level and high-level semantic information within the detection network and consists of bottom-up and top-down schemes. The bottom-up scheme (see Fig. 3 (b)) combines the backbone and LSN features and propagates the resulting features of different levels in a feed-forward cascaded way resulting in *forward features*. We refer this task as bottom-up feature propagation (BFP). The k^{th} level forward feature is obtained by performing both tasks:

$$f_k = \phi_k((s_k \otimes o_k) \oplus (w_{k-1} f_{k-1}))) \tag{5}$$

where s_k is the k^{th} feature from LSN, o_k represents the k^{th} original SSD prediction backbone feature, w_{k-1} denotes a 3×3 conv. block (without ReLU) with a stride of 2, f_{k-1} is the forward feature from the $(k-1)^{th}$ level and $\phi_k(.)$ denotes serial operations including ReLU and 3×3 conv. block. $\otimes$ and $\oplus$ denote element-wise multiplication and addition, respectively. Note that BFP starts from the second prediction layer. Therefore, the forward feature f_1 for the first prediction layer is in fact the fusion of the LSN and backbone features, represented as:

$$f_1 = \phi_1(s_1 \otimes o_1) \tag{6}$$

Finally, the forward features from all levels of the bottom-up scheme are represented as a forward feature pyramid:

$$F_p = \{f_1, f_2, \ldots, f_n\} \tag{7}$$

As described above, the bottom-up scheme circulates the low-/mid-level features in the forward direction. To further inject the high-level semantic information from the later to former layers, we introduce a top-down scheme (see Fig. 3 (c)). This scheme connects all the features from later layers to the current layer. It circulates high-level semantics through independent parallel connections in the network.

The backward feature pyramid B_p is generated for prediction as

$$B_p = \{b_1, b_2, \ldots, b_n\} \tag{8}$$

We first employ several 1×1 conv. blocks to reduce the feature channels of all the forward features in F_p. For k^{th} level, where $k = (1, \ldots, n-1)$, the feature with reduced channels is merged with all the higher level features to obtain the backward feature b_k for the final prediction,

$$b_k = \gamma_k(\sum(W_k f_k, W_{mk}(\sum_{k+1}^{n} \mu_k(W_i f_i)))) \tag{9}$$

where $W_i, i = (k, \ldots, n)$ is a 1×1 conv. block to reduce the feature channels. W_{mk} is a 1×1 conv. block to merge features from all the higher levels. μ_k is the upsampling operation. $\gamma_k(.)$ is a 3×3 conv. block to merge all the forward features. $\sum$ is a concatenation operation. Note that the n^{th} level forward feature is the highest level semantic feature and does not require any semantic information from former layers. This implies that the forward features of this n^{th} level are directly used as the prediction features.

4. Experiments

4.1. Datasets

MS COCO [19]: contains 80 object categories. It consists of 160k images in total, with 80k training, 40k validation and 40k test-dev images. The training is performed on 120k images from the trainval set and evaluation is done on the test-dev images. Here, the performance is evaluated by following the standard MS COCO protocol where average precision (AP) is measured by averaging over multiple IOU thresholds, ranging from 0.5 to 0.95.

UAVDT dataset [9]: is a recently introduced large-scale benchmark for object detection. The object of interest in this benchmark is *vehicle*. The vehicle category consists of car, truck and bus. The dataset contains 80k annotated frames selected from 100 video sequences. The videos are divided into training and testing sets with 30 and 70 sequences, respectively. We follow the same evaluation protocol provided by the respective authors [9].

4.2. Implementation Details

We employ VGG-16 [32], pre-trained on ImageNet [30] as the backbone architecture in all baseline and UAVDT experiments. In addition to VGG, we also report results with ResNet-101 backbone on MS COCO dataset. Note that our approach does not require any significant redesigning of the underlying architecture, with change in backbone. When going from VGG to ResNet backbone, only the number of channels is changed. For both datasets, we adopt a warm-up strategy for the first six epochs. The initial learning rate is set to 2×10^{-3} and gradually decreased to 2×10^{-4} and 2×10^{-5} at 90 and 120 epochs, respectively. We employ the default settings as in the standard SSD method [21] for loss function, scales and aspect ratios of the defaults boxes and data augmentation. In our experiments, the weight decay is set to 0.0005 and the momentum to 0.9. For both datasets, the batch-size is 32. A total number of 160 epochs are performed for both two datasets.

4.3. MS COCO Dataset

State-of-the-art Comparison: We first perform a comparison of our approach with state-of-the-art object detection methods in literature. Tab. 1 shows the comparison on MS COCO test-dev set. For a 300×300 input, the baseline SSD method obtains a detection AP score of 25.3. On large

Methods	Backbone	Input size	Time(ms)	AP	AP_{50}	AP_{75}	AP_s	AP_m	AP_l
Two-Stage Detector:									
Faster-RCNN [29]	VGG-16	$\sim 1000 \times 600$	147	24.2	45.3	23.5	7.7	26.4	37.1
Faster-FPN [17]	ResNet-101-FPN	$\sim 1000 \times 600$	240	36.2	59.1	39.0	18.2	39.0	48.2
R-FCN [7]	ResNet-101	$\sim 1000 \times 600$	110	29.9	51.9	-	10.8	32.8	45.0
Deformable R-FCN [8]	ResNet-101	$\sim 1000 \times 600$	125	34.5	55.0	-	14.0	37.7	50.3
Mask-RCNN [13]	ResNeXt-101-FPN	$\sim 1280 \times 800$	210	39.8	62.3	43.4	22.1	43.2	51.2
Cascade R-CNN [2]	ResNet-101-FPN	$\sim 1280 \times 800$	141	42.8	62.1	46.3	23.7	45.5	55.2
SNIP [33]	DPN-98	-	-	45.7	67.3	51.1	29.3	48.8	57.1
Single-Stage Detector:									
SSD [21]	VGG-16	300×300	12	25.3	42.0	26.5	6.2	28.0	43.3
SSD [10]	ResNet-101	321×321	20	28.0	45.4	29.3	6.2	28.3	49.3
DSSD [10]	ResNet-101	321×321	-	28.0	46.1	29.2	7.4	28.1	47.6
RefineDet [36]	VGG-16	320×320	26	29.4	49.2	31.3	10.0	32.0	44.4
RefineDet [36]	ResNet-101	320×320	-	32.0	51.4	34.2	10.5	34.7	50.4
RFBNet [20]	VGG-16	300×300	15	30.3	49.3	31.8	11.8	31.9	45.9
EFIP [24]	VGG-16	300×300	14	30.0	48.8	31.7	10.9	32.8	46.3
Ours	VGG-16	300×300	13	32.0	51.5	33.8	12.6	34.9	47.0
Ours	ResNet-101	300×300	19	**34.3**	**54.1**	**36.6**	**13.2**	**38.2**	**50.7**
YOLOv2 [27]	Darknet	544×544	25	21.6	44.0	19.2	5.0	22.4	35.5
YOLOv3 [28]	DarkNet-53	608×608	51	33.0	57.9	34.4	18.3	35.4	41.9
SSD [21]	VGG-16	512×512	28	28.8	48.5	30.3	10.9	31.8	43.5
SSD [10]	ResNet-101	513×513	32	31.2	50.4	33.3	10.2	34.5	49.8
DSSD [10]	ResNet-101	513×513	156	33.2	53.3	35.2	13.0	35.4	51.1
RefineDet [36]	VGG-16	512×512	45	33.0	54.5	35.5	16.3	36.3	44.3
RefineDet [36]	ResNet-101	512×512	-	36.4	57.5	39.5	16.6	39.9	51.4
Rev-Dense [35]	VGG-16	512×512	-	31.2	52.9	32.4	15.5	32.9	43.9
RFBNet [20]	VGG-16	512×512	30	33.8	54.2	35.9	16.2	37.1	47.4
RFBNet-E [20]	VGG-16	512×512	33	34.4	55.7	36.4	17.6	37.0	47.6
RetinaNet [18]	ResNet-101-FPN	$\sim 832 \times 500$	90	34.4	55.7	36.8	14.7	37.1	47.4
EFIP [24]	VGG-16	512×512	29	34.6	55.8	36.8	18.3	38.2	47.1
RetinaNet+AP-Loss [5]	ResNet-101-FPN	$\sim 832 \times 500$	91	**37.4**	**58.6**	**40.5**	17.3	40.8	**51.9**
Ours	VGG-16	512×512	26	36.2	56.6	38.7	19.0	39.9	48.8
Ours	ResNet-101	512×512	32	37.3	58.5	39.7	**19.7**	**42.8**	50.1

Table 1: Comparison (in terms of AP) of our detector with state-of-the-art methods on MS COCO test-dev set. Our approach achieves impressive performance for both 300×300 and 512×512 inputs. When using a 300×300 input, our detector with ResNet-101 backbone surpasses existing single-stage methods in terms of overall accuracy while operating at an inference time of 19 milliseconds (ms). Our detector also outperforms existing single-stage methods on both small and medium objects.

objects (AP_l), the baseline SSD provides a decent performance of 43.3 AP. However, its performance significantly deteriorates to 6.2 AP on small objects (AP_s). Our approach, using the same VGG backbone, provides a significant overall gain of 6.7% in detection AP over the baseline SSD. Importantly, our detector achieves more than double the detection performance on small objects, compared to the SSD framework. Similarly, a large improvement in detection performance is also obtained on medium objects (AP_m). Among existing methods, RefineDet [36] and RFBNet [20] with VGG backbone achieve AP scores of 29.4 and 30.3, respectively. Our detector with the same backbone achieves superior results compared to both these methods.

For a 512×512 input, the baseline SSD achieves a detection AP score of 28.8. Our detector with same VGG backbone provides a significant overall gain of 7.4% in AP, over the baseline SSD. Among existing methods, RetinaNet [18] and RetinaNet+AP-Loss [5] provide detection AP scores of 34.4 and 37.4, respectively. However, both approaches are slower with inference times of $\sim$ 90ms. Our approach with the same ResNet-101 backbone (without FPN) achieves comparable performance with a detection AP score of 37.3, while operating at significantly faster inference time of 32 millisecond (ms) on a single Titan X GPU.

Although two-stage methods achieve superior accuracy, they are computationally expensive, often require a large input resolution and mostly take more than 100ms to process an image. For instance, Cascade R-CNN [2] achieves 42.8 AP but requires 141ms to process an image. Our detector provides promising accuracy with high time efficiency.

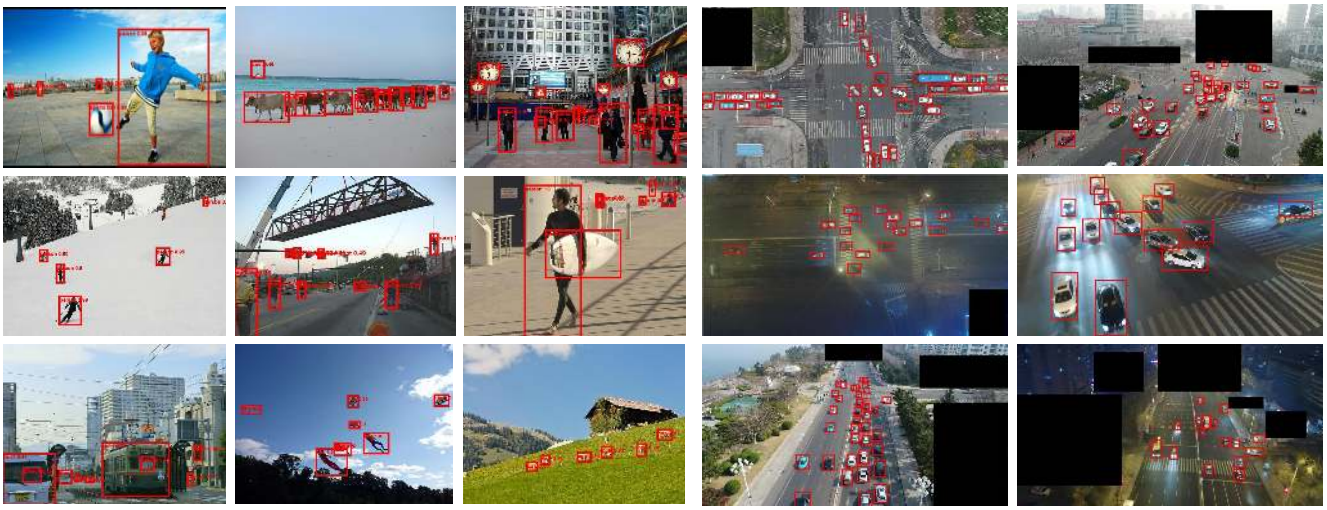

a: COCO detection results b: UAVDT detection results

Figure 5: Qualitative detection results of our approach on (a) COCO test-dev (corresponding to 36.2 AP) and (b) UAVDT test set (corresponding to 37.8 AP). Most of examples depict the performance on small objects. The black regions are ignored in UAVDT dataset images [9]. Our detector is able to accurately localize small objects in these challenging scenes.

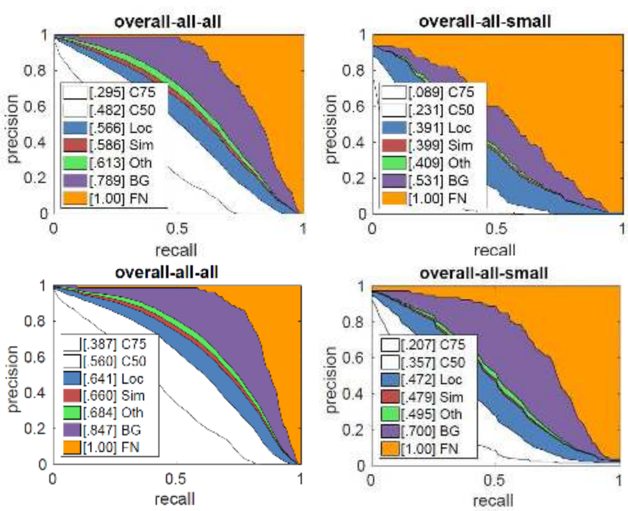

Figure 6: Error analysis comparison between the baseline SSD (top row) and our detector (bottom row). The comparison is shown for both overall and small sized objects. Each sub-image contains plots that describe a series of precision recall curves computed using different evaluation settings [19]. Further, the area under each curve is presented (brackets) in the legend. Our approach significantly improves the detection performance over the baseline SSD framework.

Qualitative Analysis: A large number of small sized objects (41% of all objects) in the MS COCO dataset makes it especially suitable to evaluate the performance for small object detection. An object instance is considered small here if the area is $< 32^2$. We perform a further analysis of our detector by employing the error analysis protocol provided by [19]. The error analysis plots of the baseline SSD (top row) and our approach (bottom) with VGG backbone for both overall and small objects are shown in Fig. 6. As defined by [19], the plots in each sub-image depict a series of precision recall curves employing different settings. The area under each curve is shown (brackets) in the legends. In case of the baseline SSD (top row), the overall AP at IoU=0.50 is 0.482 and removing the background false positives will result in improving the performance to 0.789 AP. For our approach (bottom row), the overall AP at IoU=0.50 is 0.560 and removing the background false positives will increase the performance to 0.847 AP. In case of small sized objects, our approach provides more notable improvements in performance, compared to SSD. For instance, the results are significantly improved from 0.231 obtained by SSD to 0.357 at IoU=0.50 for our method. Further, Fig. 5 (a) shows detection examples with our approach.

Ablation Study: We perform an ablation study on the MS COCO-minival and report results using a 300×300 input with VGG backbone. We first validate the impact of our proposed components: light-weight scratch network (LSN) (sec. 3.1) and bi-directional network (sec. 3.2). Note that our bi-directional network consists of bottom-up and top-down schemes to circulate both low-/mid-level and high-levelsemantic information within the detection network. Tab. 2 shows the impact of our LSN and bi-directional network. The standard SSD provides a detection AP score of 25.3. Integrating our LSN significantly improves the detection performance with AP score of 28.9. Notably, a significant gain of 4.4% is obtained compared to the baseline SSD for small sized objects (AP$_s$). The large gain in performance especially for small (AP$_s$) and medium (AP$_m$) objects shows the impact of our LSN on compensating for the

SSD	LSN	Bi-directional	AP	AP_{50}	AP_{75}	AP_s	AP_m	AP_l
✓			25.3	42.0	26.5	6.2	28.0	43.3
✓	✓		28.9	47.8	30.2	10.6	32.1	44.8
✓	✓	✓	**31.9**	**51.4**	**33.6**	**13.4**	**36.3**	**47.6**

Table 2: Impact of integrating our different components (light-weight scratch network (LSN) and bi-directional network) in the standard SSD on MS COCO minival dataset. Our final detection framework improves the performance with an overall gain of 6.6% over the standard SSD.

Bottom-up Scheme	Top-down Scheme	AP	Time (ms)
Cascade	Cascade	31.0	**12**
Dense	Dense	31.3	16
Dense	Cascade	29.6	15
Cascade	Dense	**31.9**	13

Table 3: Impact of different design choices when constructing our bi-directional network. We obtain optimal performance in terms of speed and accuracy when using cascade connections for bottom-up scheme and dense connections for top-down scheme in our bi-directional network.

loss of information in the standard SSD backbone features. Further, integrating our bi-directional network improves the overall performance from 28.9 to 31.9. The bottom-up and top-down schemes in our bi-directional network provide improvements of 1% and 2%, respectively.

We also perform an experiment by integrating our LSN features at different stages of the SSD backbone. A large gain of 2.2% is obtained when injecting LSN features at the $conv4\_3$ level. Importantly, a large improvement of 3.8% is obtained for small sized objects (AP_s) demonstrating the importance of compensating loss of information in the standard backbone features. Moreover, we observe a gradual increase in performance when injecting LSN features to higher layers. We also perform an experiment by re-using the $conv1$ layer of the backbone in the standard SSD, instead of our LSN, to generate complementary features. However, the re-usage of shallow backbone features achieves inferior results (26.8 AP) compared to our LSN (28.9 AP) highlighting the importance of using features exclusively trained from scratch. Finally, we compare our top-down scheme in bi-direcional network with the top-down pyramid representation used in FPN. Integrating top-down scheme of FPN in standard SSD (SSD-FPN) provides an AP score of 27.3. An additional absolute gain of 2% is obtained with an AP score of 29.3, when integrating our top-down scheme in standard SSD, compared to SSD-FPN.

Tab. 3 shows the analysis of different design choices taken into consideration during the construction of our bi-directional network. We report both overall detection performance and inference time when integrating the bi-directional network into the standard SSD (without LSN). When using a cascade connection for both bottom-up and top-down schemes, we obtain an optimal speed but at the cost of reduced accuracy. On the other hand, using dense connections for both bottom-up and top-down schemes increases the computational overhead. Optimal performance in terms of speed and accuracy is obtained when using cascade connections for bottom-up scheme and dense connections for top-down scheme. Therefore, we select this design choice for the construction of our bi-directional network.

Methods	Backbone	input size	AP	FPS
Faster-RCNN [29]	VGG-16	1024 × 540	22.32	2.8
R-FCN [7]	ResNet-50	1024 × 540	34.35	4.7
SSD [21]	VGG-16	512 × 512	33.62	120.0
RON [16]	VGG-16	512 × 512	21.59	11.1
RetinaNet [18]	ResNet-101-FPN	512 × 512	33.95	25.0
Ours	VGG-16	512 × 512	37.81	91.0

Table 4: Speed and performance comparison of our detector with several existing single and two-stage methods on UAVDT test set. For fair comparison, the speed for all methods is measured on a single Titan X GPU (Maxwell architecture). Best two results are shown in red and blue, respectively. Our approach improves the accuracy by 3.5% in AP, while providing a nearly 20-fold speedup over R-FCN.

4.4. Unmanned Aerial Vehicle Dataset

Finally, we validate our detector on Unmanned Aerial Vehicle (UAVDT) dataset [9]. The UAVDT dataset is extremely challenging due to, *e.g.*, high density, small object, and camera motion. Note that we follow the protocol provided by [9] and evaluate the performance using the PASCAL style AP. Tab. 4 shows a comparison with several existing single and two-stage detectors. In case of Faster-RCNN [29], R-FCN [7], SSD [21] and RON [16], the results are taken from [9]. In addition to these detectors, we evaluate the single-stage RetinaNet [18] using the publicly available code provided by the respective authors. Among single-stage methods, SSD and RetinaNet provide detection scores of 33.62 and 33.95, respectively. The best result is achieved by the two-stage R-FCN [7], with an AP score of 34.35. Our detector outperforms R-FCN with an AP score of 37.81, while providing nearly a 20-fold speedup. Fig. 5 (b) shows detection examples for our approach.

5. Conclusion

We propose a single-stage object detection approach with three components: a standard SSD network, a light-weight scratch network (LSN) and a bi-directional network. Our LSN is trained from scratch yielding features that are complementary to the standard backbone features. The bi-directional network is designed to circulate both low-/mid-level and high-level semantic information within the detection network. Experiments on two challenging detection datasets show that our approach achieves superior results with high time efficiency.

Acknowledgments: This work is supported by the National Natural Science Foundation of China (Grant # 61632018).

References

[1] Yancheng Bai, Yongqiang Zhang, Mingli Ding, and Bernard Ghanem. Sod-mtgan: Small object detection via multi-task generative adversarial network. In *ECCV*, 2018. 2

[2] Zhaowei Cai and Nuno Vasconcelos. Cascade r-cnn: Delving into high quality object detection. In *CVPR*, 2018. 6

[3] Jiale Cao, Yanwei Pang, Jungong Han, and Xuelong Li. Hierarchical shot detector. In *ICCV*, 2019. 1

[4] Jiale Cao, Yanwei Pang, and Xuelong Li. Triply supervised decoder networks for joint detection and segmentation. In *CVPR*, 2019. 1, 2

[5] Kean Chen, Jianguo Li, Weiyao Lin, John See, Ji Wang, Lingyu Duan, Zhibo Chen, Changwei He, and Junni Zou. Towards accurate one-stage object detection with ap-loss. In *CVPR*, 2019. 6

[6] Hisham Cholakkal, Guolei Sun, Fahad Shahbaz Khan, and Ling Shao. Object counting and instance segmentation with image-level supervision. In *CVPR*, 2019. 1

[7] Jifeng Dai, Yi Li, Kaiming He, and Jian Sun. R-FCN: Object detection via region-based fully convolutional networks. In *NIPS*, 2016. 6, 8

[8] Jifeng Dai, Haozhi Qi, Yuwen Xiong, Yi Li, Guodong Zhang, Han Hu, and Yichen Wei. Deformable convolutional networks. In *ICCV*, 2017. 6

[9] Dawei Du, Yuankai Qi, Hongyang Yu, Yifan Yang, Kaiwen Duan, Guorong Li, Weigang Zhang, Qingming Huang, and Qi Tian. The unmanned aerial vehicle benchmark: Object detection and tracking. In *ECCV*, 2018. 1, 5, 7, 8

[10] Cheng-Yang Fu, Wei Liu, Ananth Ranga, Ambrish Tyagi, Alexander, and C. Berg. Dssd : Deconvolutional single shot detector. *arXiv preprint arXiv:1701.06659*, 2017. 2, 3, 6

[11] Ross Girshick. Fast r-cnn. In *ICCV*, 2015. 2

[12] Kaiming He, Ross Girshick, and Piotr Dollar. Rethinking imagenet pre-training. *arXiv preprint arXiv:1811.08883*, 2018. 2

[13] Kaiming He, Georgia Gkioxari, Piotr Dollar, and Ross Girshick. Mask R-CNN. In *ICCV*, 2017. 6

[14] Kaiming He, Xiangyu Zhang, Shaoqing Ren, and Jian Sun. Spatial pyramid pooling in deep convolutional networks for visual recognition. In *ECCV*, 2014. 2

[15] Jonathan Huang, Vivek Rathod, Chen Sun, Menglong Zhu, Anoop Korattikara, Alireza Fathi, Ian Fischer, Zbigniew Wojna, Yang Song, Sergio Guadarrama, and Kevin Murphy. Speed/accuracy trade-offs for modern convolutional object detectors. In *CVPR*, 2017. 2, 3

[16] Tao Kong, Fuchun Sun, Anbang Yao, Huaping Liu, Ming Lu, and Yurong Chen. Ron: Reverse connection with objectness prior networks for object detection. In *CVPR*, 2017. 8

[17] Tsung-Yi Lin, Piotr Dollar, Ross Girshick, Kaiming He, Bharath Hariharan, and Serge Belongie. Feature pyramid networks for object detection. In *CVPR*, 2017. 2, 3, 4, 6

[18] Tsung-Yi Lin, Priya Goyal, Ross Girshick, Kaiming He, and Piotr Dollr. Focal loss for dense object detection. In *ICCV*, 2017. 1, 2, 3, 4, 6, 8

[19] Tsung-Yi Lin, Michael Maire, Serge Belongie, James Hays, Pietro Perona, Deva Ramanan, Piotr Dollr, and C. Lawrence Zitnick. Microsoft coco: Common objects in context. In *ECCV*, 2014. 1, 2, 5, 7

[20] Songtao Liu, Di Huang, and Yunhong Wang. Receptive field block net for accurate and fast object detection. In *ECCV*, 2018. 2, 6

[21] Wei Liu, Dragomir Anguelov, Dumitru Erhan, Christian Szegedy, Scott Reed, Cheng-Yang Fu, and Alexander C. Berg. SSD: Single shot multibox detector. In *ECCV*, 2016. 1, 2, 4, 5, 6, 8

[22] Yanwei Pang, Jiale Cao, and Xuelong Li. Cascade learning by optimally partitioning. *IEEE Transactions on Cybernetics*, 47(12):4148–4161, 2017. 1

[23] Yanwei Pang, Manli Sun, Xiaoheng Jiang, and Xuelong Li. Convolution in convolution for network in network. *IEEE Transactions on Neural Networks and Learning System*, 29(5):1587–1597, 2018. 1

[24] Yanwei Pang, Tiancai Wang, Rao Muhammad Anwer, Fahad Shahbaz Khan, and Ling Shao. Efficient featurized image pyramid network for single shot detector. In *CVPR*, 2019. 2, 3, 6

[25] Yanwei Pang, Jin Xie, and Xuelong Li. Visual haze removal by a unified generative adversarial network. *IEEE Transactions on Circuits and Systems for Video Technology*, 2018. 1

[26] Joseph Redmon, Santosh Divvala, Ross Girshick, and Ali Farhadi. You only look once: Unified, real-time object detection. In *CVPR*, 2016. 1

[27] Joseph Redmon and Ali Farhadi. Yolo9000:better, faster, stronger. In *CVPR*, 2017. 1, 6

[28] Joseph Redmon and Ali Farhadi. Yolov3: An incremental improvement. *arXiv preprint arXiv:1804.02767*, 2018. 1, 2, 6

[29] Shaoqing Ren, Kaiming He, Ross Girshick, and Jian Sun. Faster R-CNN: towards real-time object detection with region proposal networks. In *NIPS*, 2015. 2, 6, 8

[30] Olga Russakovsky, Jia Deng, Hao Su, Jonathan Krause, Sanjeev Satheesh, Sean Ma, Zhiheng Huang, Andrej Karpathy, Aditya Khosla, Michael Bernstein, Alexander C. Berg, and Li Fei-Fei. Imagenet large scale visual recognition challenge. In *IJCV*, 2015. 2, 5

[31] Fahad Shahbaz Khan, Xu Jiaolong, Joost van de Weijer, Andrew Bagdanov, and Antonio Anwer, Rao Muhammad Lopez. Recognizing actions through action-specific person detection. *IEEE Transactions on Image Processing*, 24(11):4422–4432, 2015. 2

[32] Karen Simonyan and Andrew Zisserman. Very deep convolutional networks for large-scale image recognition. In *NIPS*, 2014. 5

[33] Bharat Singh and Larry Davis. An analysis of scale invariance in object detection - snip. In *CVPR*, 2018. 6

[34] Hanqing Sun and Yanwei Pang. Glancenets-efficient convolutional neural networks with adaptive hard example mining. *SCIENCE CHINA Information Sciences*, 61(10), 2018. 1

[35] Yongjian Xin, Shuhui Wang, Liang Li, Weigang Zhangg, and Qingming Huang. Reverse densely connected feature pyramid network for object detection. In *ACCV*, 2018. 3, 6

[36] Shifeng Zhang, Longyin Wen, Xiao Bian, Zhen Lei, and Stan Z. Li. Single-shot refinement neural network for object detection. In *CVPR*, 2018. 2, 4, 6

[37] Zhishuai Zhang, Siyuan Qiao, Cihang Xie, Wei Shen, Bo Wang, and Alan Yuille. Single-shot object detection with enriched semantics. In *CVPR*, 2018. 3

[38] Rui Zhu, Shifeng Zhang, Xiaobo Wang, Longyin Wen, Hailin Shi, Liefeng Bo, and Tao Mei. Scratchdet: Training single-shot object detectors from scratch. In *CVPR*, 2019. 2, 4